Simulation of the weakly nonlinear propagation in a straight pipe: application to a real-time brassy audio effect

Thomas Hélie* and Vanessa Smet†

***Abstract*— Nonlinear propagation in acoustic pipes is responsible for the brightness of the brass sounds at fortissimo nuances. Using the formalism of Volterra series, an acoustic model of this phenomenon is solved as an input-output system. An identification of the Volterra kernels leads to a structure composed of linear filters, sums, and instantaneous products of signals. A digital simulation which guarantees no aliasing is derived, from which real-time versions have been implemented.**

***Index Terms*— Volterra series, Nonlinear acoustics, Signal processing, Real-time audio systems**

I. INTRODUCTION

The so-called "brassy effect" refers to the brightness of the sound of brass musical instruments at *fortissimo* nuances. This phenomenon is due to an audible distortion which comes from the nonlinear propagation in sufficiently long acoustic pipes for sufficiently large pressure amplitudes (see e.g. [1]). Such a problem can be analytically solved for standing waves [2]. In [3], Volterra series proved to be relevant to tackle the case of non stationary waves.

In this paper, both an academic and a more realistic Burgers model are analyzed using the Volterra series. An identification procedure performed on the kernels leads to realizable structures. For the academic example, this procedure is straightforward. On the contrary, for the realistic acoustic model which involves irrational Volterra kernels, a special algebraic decomposition is required. From the application point of view, this decomposition is crucial since it gives the precise link between some formal Volterra kernels and a realizable structure composed of linear filters, sums, and instantaneous products. Then, a digital version which simulates the Volterra kernels of orders 1 and 2, and which rejects aliasing, is derived. Straightforward real-time versions can be implemented to simulate artificial audio brassy effects, or can be embedded into a complete model of brass instruments.

The paper is structured as follows. In section II the acoustic models are described. Section III introduces the Volterra series. In section IV the Volterra kernels which solve the acoustic models are derived. Section V details the identification procedure to obtain a realizable structure. Section VI presents a low-cost digital simulation in the time domain. Finally, conclusions are given in section VII.

A part of this work has been supported by the CONSONNES project, ANR-05-BLAN-0097-01

* IRCAM-CNRS UMR 9912, 1, place Igor Stravinsky, 75004 Paris, France thomas.helie@ircam.fr

† Institut d'Electronique Sud, Université de Montpellier 2, F-34095 Montpellier cedex 5, France. vanessa.smet@ies.univ-montp2.fr

Vanessa Smet carried out this work at IRCAM-CNRS UMR 9912 during her Master's at the Ecole Normale Supérieure de Cachan, Dept. EEA.

II. ACOUSTIC MODELS

A. Burgers equation and brass instruments

The nonlinear propagation of an acoustic simple plane wave can be modeled by the so-called Burgers equation (see [2]):

$$\partial_x p + A(p) = \frac{\beta}{2c_0}\partial_\tau p^2 \tag{1}$$

where p is the pressure, x is the space variable, t is the time variable, $\tau = t - x/c_0$ is the retarded time, c_0 is celerity, A is an operator modeling the absorption mechanisms (see e.g. [2, Tab.4.3]), and β is the nonlinearity parameter. Typical values for the air are given in table I.

The simplest absorption model is independent of the frequency [2, Tab. 4.3-1]). It corresponds to

$$A_0(p) = \alpha_0\, p, \tag{2}$$

where $\alpha_0 \geq 0$ is the damping coefficient. In a straight pipe, the absorption is mainly due to the visco-thermal losses at the wall [2, Tab. 4.3-4]. It corresponds to

$$A_1(p) = \alpha_1\, \partial_\tau^{1/2} p \tag{3}$$

where a realistic damping coefficient $\alpha_1 \geq 0$ is given in table I. The fractional derivative $\partial_\tau^{1/2}$ can be understood as a multiplication in the Laplace domain by $\sqrt{s}$ with the choice $s = \rho e^{i\theta} \mapsto \sqrt{s} = \sqrt{\rho} e^{i\theta/2}$, $\rho \geq 0$, $\theta \in [-\pi, \pi[$, which is analytic on $\mathbb{C}_0^+ = \{s \in \mathbb{C} \,|\, \Re\mathrm{e}(s) > 0\}$ (see [4] for a detailed presentation).

Geometry	Coefficients of models	Physical constants
$L = 4\,\mathrm{m}$	$c_0 = \sqrt{\frac{\gamma P_0}{\rho_0}} \approx 344\,\mathrm{m.s^{-1}}$	$P_0 \approx 1.013\times10^5\,\mathrm{Pa}$
$R = 5.6\times10^{-3}\,\mathrm{m}$	$\beta = \frac{\gamma+1}{2\gamma P_0} \approx 8.46\times10^{-6}\,\mathrm{Pa^{-1}}$	$\rho_0 \approx 1.2\,\mathrm{Kg.m^{-3}}$
		$\gamma \approx 1.4$
	$\alpha_1 = a/R \approx 2.97\times10^{-3}\,\mathrm{s^{1/2}.m^{-1}}$	$a \approx 1.66\times10^{-5}\,\mathrm{s^{1/2}}$

TABLE I

Geometrical constants and coefficients used for the simulation. The coefficients are deduced from typical air constants: P_0, ρ_0, γ denote the atmospheric pressure, the mass density, and the specific heat ratio, respectively. The loss coefficient $a = \frac{\sqrt{\nu}}{c_0}\left(1 + \frac{\gamma-1}{\sqrt{P_r}}\right)$ is computed for the kinematic viscosity $\nu \approx 1.5\times10^{-5}\,m^2.s^{-1}$ and the Prandtl number $P_r \approx 0.7$.

For typical musical nuances, the pressure inside the pipe of brass instruments is such that $|p|_{dB} \leq 160\,\mathrm{dB}_{SPL}$. In [1], a dimensional analysis shows that, in this range, the acoustics of straight pipes of length L can be approximated by adding an outwardly directed wave governed by (1,3) to an inwardly directed wave (model straightforwardly deduced by symmetry, through the change of variable $\tilde{x} = L - x$).

B. Problem statement and adimensional models

In this paper, the study is focused on the nonlinear propagation of an outwardly directed wave. The fluid is assumed to be at rest before $t=0$ and the pressure at $x=0$ is a given bounded signal $p_0(t)$. Both models A_0 (academic and illustrative) and A_1 (relevant for brass instruments) are studied. Adimensional versions (with no retarded time) of these problems are derived from (1-3) using the change of variables given in Tab. II. They are given by, for $k=0$ and $k=1$:

$$\forall \widetilde{x}>0, \forall t>0, \quad \partial_{\widetilde{x}}\widetilde{p}+\partial_{\widetilde{t}}\widetilde{p}+\widetilde{\alpha}_k\partial_{\widetilde{t}}^{k/2}\widetilde{p}=\frac{\widetilde{\beta}}{2}\partial_{\widetilde{t}}\widetilde{p}^2, \tag{4}$$

$$\widetilde{x}>0, \qquad \widetilde{p}(\widetilde{x},\widetilde{t}=0)=0, \tag{5}$$

$$\forall \widetilde{t}>0, \qquad \widetilde{p}(\widetilde{x}=0,\widetilde{t})=\widetilde{p}_0(\widetilde{t}). \tag{6}$$

For sake of legibility, the tilde symbols are omitted in the following.

Variables	Functions	Constants/Coefficients
$\widetilde{x}=\frac{x}{c_0T_0}$	$\widetilde{p}(\widetilde{x},\widetilde{t})=\frac{p(x=c_0T_0\widetilde{x},\,t=T_0(\widetilde{t}-\widetilde{x}))}{P_0}$	$\widetilde{\alpha}_0=c_0T_0\,\alpha_0$
$\widetilde{t}=\frac{t}{T_0}=\frac{\tau+x/c_0}{T_0}$	$\widetilde{p}_0(\widetilde{t})=\frac{p_0(t=\frac{\widetilde{L}}{c_0})}{P_0}$	$\widetilde{\alpha}_1=c_0\sqrt{T_0}\,\alpha_1\approx 1.022$
$\widetilde{s}=T_0s$	$\widetilde{L}=\frac{L}{c_0T_0}\approx 1.16\times10^{-2}$	$\widetilde{\beta}=P_0\beta\approx 0.857$

TABLE II

Changes of variables, of functions, and of coefficients (dimensionless quantities). s denotes the Laplace variable. All numerical values are computed with those given in Tab. I and $T_0=1\,s$.

III. INTRODUCTION TO VOLTERRA SERIES

A. Definitions and notations

A system is defined by a Volterra series of kernels $\{h_n\}_{n\in\mathbb{N}^*}$ for inputs $|u|<\rho$ if the output y is given by the multi-convolutions

$$y(t)=\sum_{n=1}^{+\infty}\int_{\mathbb{R}^n} h_n(\tau_{1:n})\,u(t-\tau_1)\dots u(t-\tau_n)\,\mathrm{d}\tau_{1:n}, \tag{7}$$

denoting $(\tau_{1:n})=(\tau_1,\tau_2,\dots,\tau_n)$ and $\mathrm{d}\tau_{1:n}=\mathrm{d}\tau_1\,\mathrm{d}\tau_2\dots\mathrm{d}\tau_n$, where ρ is the convergence radius of the *characteristic function* $\varphi_h(x)=\sum_{n=1}^{+\infty}\|h_n\|_1 x^n$ and $\|h_n\|_1=\int_{\mathbb{R}^n}|h_n(\tau_{1:n})|\,\mathrm{d}\tau_{1:n}$ is the L^1-norm of h_n.

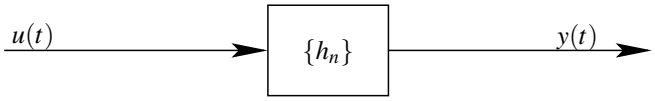

Fig. 1. *System represented by Volterra kernels*

For causal systems, h_n are zero for $\tau_k<0$. Their mono-lateral Laplace transforms [5, (29.1.2)] are denoted with capital letters

$$H_n(s_{1:n})=\int_{(\mathbb{R}^+)^n} h_n(\tau_{1:n})\mathrm{e}^{-(s_1\tau_1+s_2\tau_2+\dots+s_n\tau_n)}\,\mathrm{d}\tau_{1:n}. \tag{8}$$

For stable systems, H_n are analytic for $(s_{1:n})\in\left(\mathbb{C}_0^+\right)^n$.

Remark 1: Volterra series embed systems described by: (a) linear filters ($h_n=0$ for $n\geq 2$); (b) instantaneous nonlinear functions $y=h(u)$ with $h(0)=0$ which admits a series expansion $h(u)=\sum_{n=1}^{+\infty}c_nu^n$; (c) their various combinations (sum, product, cascade, as detailed in § III-B).

B. Interconnection laws

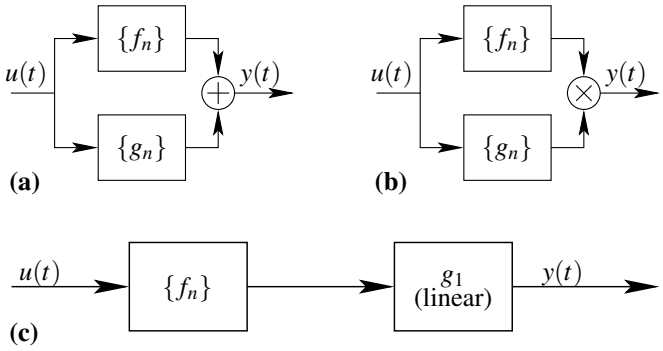

Fig. 2. *Sum (a), product (b), and cascade (c) of two systems*

The kernels $\{H_n\}_{n\in\mathbb{N}^*}$ of the systems in Figures 2a, 2b, and 2c are given respectively by [6, p. 34,35]

$$H_n(s_{1:n}) = F_n(s_{1:n})+G_n(s_{1:n}), \tag{9}$$

$$H_n(s_{1:n}) = \sum_{p=1}^{n-1}F_p(s_{1:p})G_{n-p}(s_{p+1:n}), \tag{10}$$

$$H_n(s_{1:n}) = F_n(s_{1:n})\,G_1(\widehat{s_{1:n}}), \tag{11}$$

where $\widehat{s_{1:n}}=s_1+s_2+\dots+s_n$. The radii of convergence are such that $\rho_h\geq\min(\rho_f,\rho_g)$ with $\rho_g=\infty$ for the case **(c)** if $g_1\in L^1$.

IV. VOLTERRA KERNELS OF THE BURGERS PROBLEMS

Let $\{h_n^{x,k}\}_{n\in\mathbb{N}^*}$ denote the x-parameterized Volterra kernels which solve (4-6) for $k\in\{0,1\}$.

A. Equation satisfied by the kernels

Cascading this system with the operator $\mathscr{C}:X\mapsto\partial_xX+\partial_tX+\alpha_k\partial_t^{k/2}X-\frac{\beta}{2}\partial_tX^2$ defines the *null system* (see Fig.3). Writing the kernels of this system from $\{h_n^{x,k}\}_{n\in\mathbb{N}^*}$ and $\mathscr{C}$

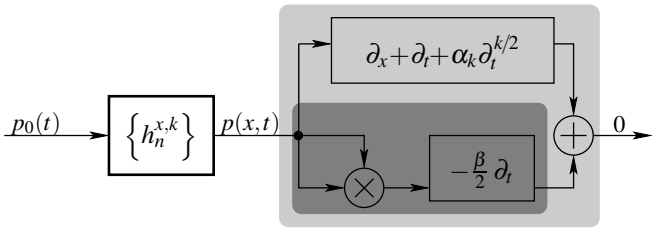

Fig. 3. *Equation (4) is described through a block-diagram involving the solution kernels. The global system is zero: all its Volterra kernels are zero.*

using (9-11) yields, in the Laplace domain, for all $n\in\mathbb{N}^*$,

$x \in]0,1[$, $(s_{1:n}) \in \left(\mathbb{C}_0^+\right)^n$,

$$\partial_x H_n^{x,k}(s_{1:n}) + \left[\widehat{s_{1:n}} + \alpha_k \left(\widehat{s_{1:n}}\right)^{\frac{k}{2}}\right] H_n^{x,k}(s_{1:n}) - \frac{\beta}{2}\widehat{s_{1:n}} \sum_{p=1}^{n-1} H_p^{x,k}(s_{1:p}) H_{n-p}^{x,k}(s_{p+1:n}) = 0, \quad (12)$$

where, for $k=1$, the square-root is defined as in § II-A.

Now, writing from (6) that $\{h_n^{x,k}\}_{n\in\mathbb{N}^*}$ defines the identity system at $x=0$ yields the boundary conditions

$$H_1^{x=0,k}(s_1) = 1, \quad \forall s_1 \in \mathbb{C}_0^+ \quad (13)$$

$$H_n^{x=0,k}(s_{1:n}) = 0, \quad \forall (s_{1:n}) \in \left(\mathbb{C}_0^+\right)^n, \text{ if } n \geq 2. \quad (14)$$

For each $n \in \mathbb{N}^*$, (12) is a linear differential equation in $H_n^{x,k}$ with respect to x which is loaded by kernels of order $p<n$.

At this step, the nonlinear boundary problem (4-6) has been transformed into a sequence (for $n \in \mathbb{N}^*$) of linear differential equations (12-14), in the Laplace domain.

B. General solution

The solution of (12-14) is given by

$$H_n^{x,k}(s_{1:n}) = G_n^{x,k}(s_{1:n})\, \mathrm{e}^{-x\widehat{s_{1:n}}}, \quad (15)$$

where

$$G_1^{x,k}(s_{1:n}) = \mathrm{e}^{-\alpha_k s_1^{\frac{k}{2}}}, \text{ if } n=1 \quad (16)$$

$$G_n^{x,k}(s_{1:n}) = \frac{\beta}{2}\widehat{s_{1:n}} \sum_{p=1}^{n-1} \int_0^x \mathrm{e}^{-\alpha_k \left(\widehat{s_{1:n}}\right)^{\frac{k}{2}}(x-\xi)} G_p^{\xi,k}(s_{1:p}) \cdot G_{n-p}^{\xi,k}(s_{p+1:n})\, \mathrm{d}\xi, \text{ if } n \geq 2. \quad (17)$$

In (15), $\mathrm{e}^{-x\widehat{s_{1:n}}}$ and $G_n^{x,k}$ account for the propagation delay and the effect due to absorption, respectively. Closed-form solutions of kernels $G_n^{x,k}$ can be derived from the recursive formula (16-17). They are proven to be analytic in $(\mathbb{C}_0^+)^n$, following the method presented in [3].

C. Truncated series and practical considerations

No results on the convergence of the series are given here: such results are available for quadratic finite dimensional systems (see [7]) but must still be generalized to infinite dimensional ones to tackle this problem presented here.

Nevertheless, the nonlinear phenomenon modelled by the Burgers equation is a cumulative one: a distortion is perceptible only if both the amplitude of the wave and the length of the pipe are sufficiently high. Hence, from a practical point of view, truncating the series at order $N=2$ is a good nonlinear approximation if the nonlinearity is weakly activated, e.g. for sufficiently short lengths L. Otherwise, because the phenomenon is cumulative, cascading M second order approximations of pipes with small lengths L/M is a practical alternative to increasing the order of truncation N.

The first kernels $G_{n=1,2}^{x,k}$ are given by, for all $(s_{1:2}) \in (\mathbb{C}_0^+)^2$,

$$G_1^{x,0}(s_1) = \mathrm{e}^{-\alpha_0 x} \quad (18)$$

$$G_2^{x,0}(s_{1:2}) = \frac{\beta\,\widehat{s_{1:2}}}{2\alpha_0}\left(1-\mathrm{e}^{-\alpha_0 x}\right) \quad (19)$$

for the simple absorption model ($k=0$), and by

$$G_1^{x,1}(s_1) = \mathrm{e}^{-\alpha_1 x\sqrt{s_1}}, \quad (20)$$

$$G_2^{x,1}(s_{1:2}) = \frac{\beta\widehat{s_{1:2}}}{2\alpha_1} \frac{\mathrm{e}^{-\alpha_1 x\sqrt{s_1+s_2}} - \mathrm{e}^{-\alpha_1 x\left(\sqrt{s_1}+\sqrt{s_2}\right)}}{-\sqrt{s_1+s_2}+\sqrt{s_1}+\sqrt{s_2}} \quad (21)$$

for the case of realistic visco-thermal losses ($k=1$).

V. IDENTIFICATION OF REALIZABLE STRUCTURES

Remark: *Results given in this section correspond to adimensional models. Their dimensional versions can be straightforwardly deduced using the changes of variables given in Tab. II.*

Low-cost simulations cannot be achieved using digital versions of the multi-convolutions in (7). To cope with this problem, kernels are identified with structures composed of linear filters, sums and instantaneous products. This process is detailed below for orders $n=1$ and $n=2$ (see e.g. [8], [9] for higher order examples).

A. General considerations

From (11), (15), and Fig. 15, the system corresponding to the truncated Volterra series $\{h_n^{x,k}\}_{n=1,2}$ can be realized using $\{g_n^{x,k}\}_{n=1,2}$ and a delay line, as described in Fig. 4. In

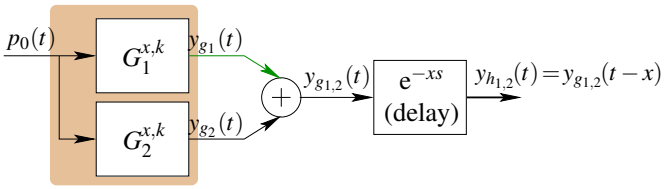

Fig. 4. Realization of $\{h_n^{x,k}\}_{n=1,2}$ from $\{g_n^{x,k}\}_{n=1,2}$ and a delay line.

this figure, kernel $G_1^{x,k}$ is the transfer function of a linear filter. Kernel $G_2^{x,k}$ can be identified with sums of elementary systems introduced below.

B. Elementary second order kernel

Consider the elementary system described in Fig.5, where P, Q, R are transfer functions of linear filters. This system

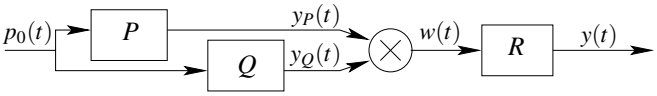

Fig. 5. Elementary triplet $P(s_1)\,Q(s_2)\,R(\widehat{s_{1:2}})$.

is nonlinear and homogeneous of degree 2. Computing its Volterra kernels K_n from (10-11) leads to null kernels, except that of order $n=2$, namely,

$$K_2(s_{1:2}) = P(s_1)\,Q(s_2)\,R(\widehat{s_{1:2}}) \quad \text{if } n=2, \quad (22)$$

$$K_n(s_{1:n}) = 0 \quad \text{otherwise.} \quad (23)$$

C. Identification of $G_2^{x,k=0}$

The kernel $G_2^{x,k=0}$ can be straightforwardly identified to (22), by choosing the triplet (P,Q,R) as follows:

$$P(s)=Q(s) \;=\; 1, \text{ (identity systems)} \tag{24}$$

$$R(s) \;=\; \frac{\beta\left(1-\mathrm{e}^{-\alpha_0 x}\right)}{2\alpha_0}s, \tag{25}$$

Note that R accounts for a static gain and a time-derivative. The block-diagram of the realization involving kernels of order 1 (see (18)) and 2 is given in Fig. 6.

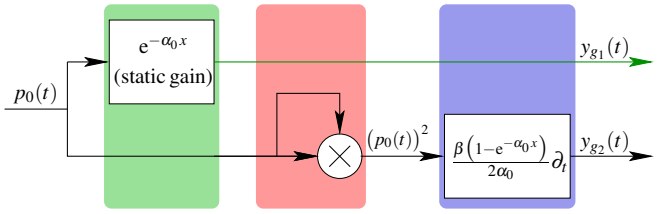

Fig. 6. Realization of $G_n^{x,0}$ with output y_{g_n} for $n=1,2$.

D. Identification of $G_2^{x,k=1}$

The case of $G_2^{x,k=1}$ is not as straightforward as the academic example $G_2^{x,k=0}$. Expanding the numerator and the denominator of $\left[\frac{\sqrt{s_1+s_2}+\sqrt{s_1}+\sqrt{s_2}}{\sqrt{s_1+s_2}+\sqrt{s_1}+\sqrt{s_2}}\cdot G_2^{x,k=1}(s_{1:2})\right]$ leads to

$$\begin{aligned} G_2^{x,k=1}(s_{1:2}) \;=\; &\Big[A(s_1)\,\mathbf{1}(s_2)\,B_x(\widehat{s_{1:2}})+\mathbf{1}(s_1)A(s_2)\,B_x(\widehat{s_{1:2}})\\ &+A(s_1)A(s_2)D_x(\widehat{s_{1:2}})\\ &-B_x(s_1)C_x(s_2)\mathbf{1}(\widehat{s_{1:2}})-C_x(s_1)B_x(s_2)\mathbf{1}(\widehat{s_{1:2}})\\ &-C_x(s_1)C_x(s_2)E(\widehat{s_{1:2}})\Big]\frac{\beta}{4\alpha_1}\widehat{s_{1:2}}, \end{aligned} \tag{26}$$

where $\mathbf{1}(s)=1$, $A(s)=1/\sqrt{s}$, $B_x(s)=G_1^{x,1}(s)=\mathrm{e}^{-\alpha_1 x\sqrt{s}}$, $C_x(s)=\mathrm{e}^{-\alpha_1 x\sqrt{s}}/\sqrt{s}$, $D(s)=\sqrt{s}\,\mathrm{e}^{-\alpha_1 x\sqrt{s}}$, and $E(s)=\sqrt{s}$ (see [10]). Note that the first and second terms of (26) define the same system, commuting A and $\mathbf{1}$. Obviously, the same applies to other pairs of terms, namely, numbers 4 and 5. Hence, from (9), $H_2^{x,1}$ can be represented with only four distinct triplets (P,Q,R) as described in Fig.7. Finally, the realization of $\{G_1^{x,1},G_2^{x,1}\}$ requires the simulation

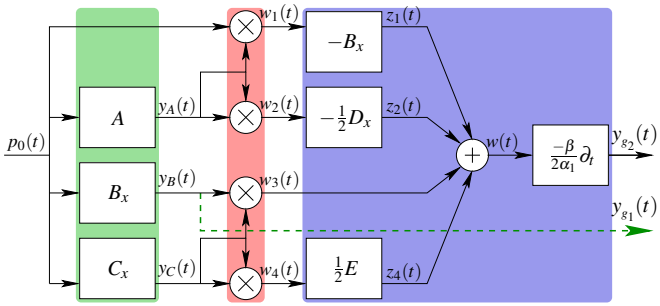

Fig. 7. Realization of $H_n^{x,1}$ with output y_{g_n} for $n=1,2$.

of six irrational transfer functions, one derivative, and four multiplications.

VI. DIGITAL SIMULATION WITHOUT ALIASING AND RESULTS

The block-diagrams in Figs. 4 and 7 involve linear filters, sums, products, a delay, and no feedback-loop. A digital version which rejects aliasing and which is well-suited to real-time applications is proposed below.

Remark: *This section presents simulations corresponding to* dimensional models *with the numerical values given in Tab. I.*

A. Transfer functions A ,B_x, C_x, D_x, E

The transfer functions A, B_x, C_x, D_x, E involved in Fig. 7 are irrational of *diffusive type*, see e.g. [11]. They correspond to well-known infinite dimensional systems, the study of which is out of the purpose of this paper. In [12], a detailed study and well-posed integral representations of these transfer functions are proposed, from which efficient low-order approximations are derived using optimization procedures in the Fourier domain (see also [13], [14]). These approximations correspond to ARMA filters with P poles and P or $P-1$ zeroes.

Here, we choose to use this method. The results summarized in Fig. 8 are obtained for the values given in Tab. I and for the following choices: $P=12$ poles for functions depending on x, $P=8$ poles for A and E, the optimization is performed on the frequency range $[0,f_s]$, and the sampling frequency is $\check{f}_s=2f_s$ with $f_s=44.1\,\mathrm{kHz}$. These approximations reveal themselves to be good overall the audible range.

B. Anti-aliasing, delay line, derivative

In the time domain, multiplying two signals with a frequency range $[0,f_{max}]$ defines a signal which is band-limited on $[0,2f_{max}]$. Such multiplications are the only nonlinearities in Fig. 7, and so, the only sources of aliasing in a discrete-time version of this realization.

In order to reject this aliasing, it is sufficient to encapsulate the discrete time version of Fig. 7 with an oversampling pre-processor and a sub-sampling post-processor of factor $\sigma=2$ so that the internal sampling frequency is $\check{f}_s=\sigma f_s=88.2\mathrm{kHz}$.

Practically, the impulse response of the low-pass anti-aliasing filters is chosen as

$$h_-(k)=\sigma\,\mathrm{sinc}\big(\pi(k-\check{K}-\eta)/\sigma\big)W_{\check{K}}(k) \tag{27}$$

where $\mathrm{sinc}(x)=\sin(\pi x)/(\pi x)$, $W_{\check{K}}$ denotes the Hanning window on $k\in[0,2\check{K}]_{\mathbb{N}}$, and $\check{K}=\sigma K$ with $K=6$. The cut-off frequency is $f_c=f_s=22.1\,\mathrm{kHz}$ (see Fig.9) and the phase is linear. The delay introduced by this filter corresponds to $\check{K}+\eta$ samples and is removed from the delay line (see Fig. 4). This is a very convenient way to to cope with fractional delays. Indeed, the exact delay due to the pipe corresponds to $\check{d}=\check{f}_sL/c_0\approx 1026.117$. We include $\eta=\check{d}-\sigma[\check{d}/\sigma]\approx 0.117$ in the low-pass filter h_- of the oversampling pre-processor.

Moreover, y_{h_1} does not require an anti-aliasing filter, so that the anti-aliasing filter of the sub-sampling post-processor is merged with the last derivative $g\partial_t$ (cf. Fig.7), where the (dimensional) gain is $g=\frac{-\beta}{2\alpha_1 P_0}\approx 4.138\,\mathrm{Pa}^{-1}$. This defines

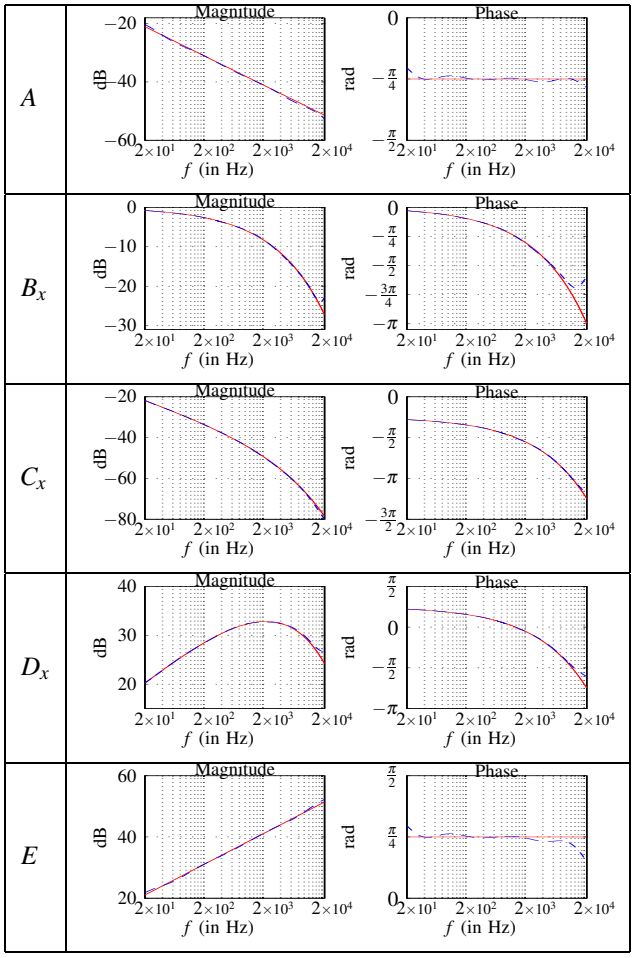

Fig. 8. Bode diagrams of A, B_x, C_x, D_x, E computed for values given in Tab. I and $x = L$. Exact responses (-) are computed from the analytic expressions given in § V-D with $s = 2i\pi f$. The dotted lines (- -) represent the frequency responses of the digital ARMA-filter approximations, obtained using the method proposed in [12].

the filter with impulse response $g\,h_+(k)$ for $k \in [0, 2\check{K}]_{\mathbb{N}}$, where

$$h_+(k) = \check{f}_s \mathrm{sinc}'\big(\pi(k-\check{K})/2\big). \tag{28}$$

The Bode diagrams corresponding to h_- and h_+ are presented on Fig. 9. These approximations reveal themselves to be good overall the audible range.

Finally, in the first stage of Fig.7, the transfer functions B_x and C_x share the same simple poles and the same input. Hence, they can be realized using a diagonal state-space representation (with a common state of dimension $P = 12$ and observation matrices with two rows). This leads to the final structure given in Fig.10.

C. Results

In Fig. 11, results are presented for a wave $p_0^{(T1)}(t)$ of sinusoidal type with a short linear attack (20 ms), a longer linear decay (0.65s) and a slowly varying frequency (vibrato around 440 Hz±5%). This quasi-sinusoidal input reveals some expected results. Due to the second order Volterra kernel, the second harmonic is activated for sufficiently high amplitude (attack, sustain) and disappears for low amplitudes

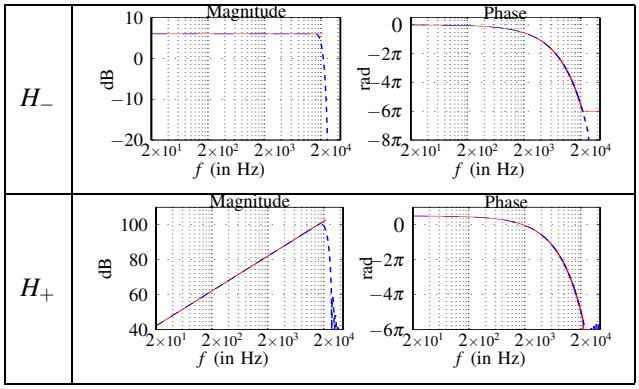

Fig. 9. *Bode diagrams of h_- and h_+. For h_-: response of an ideal low-pass filter with an ideal delay $\check{K}+\eta$ (-), and response of the approximated version (28) with $\check{K} = 2K = 12$ (- -). For h_-: response of an ideal derivative concatenated with an ideal delay $\check{K}$, and an ideal low-pass filter (-), and response (- -) of (27).*

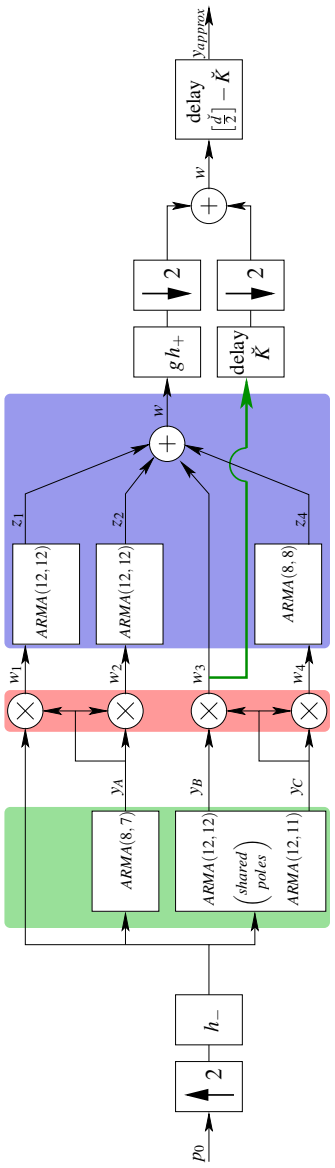

Fig. 10. Final structure of the digital simulation (algorithmic complexity is about 41 MFLOPS for the sampling frequency $\check{f}_s = 2f_s = 88.2$ kHz.

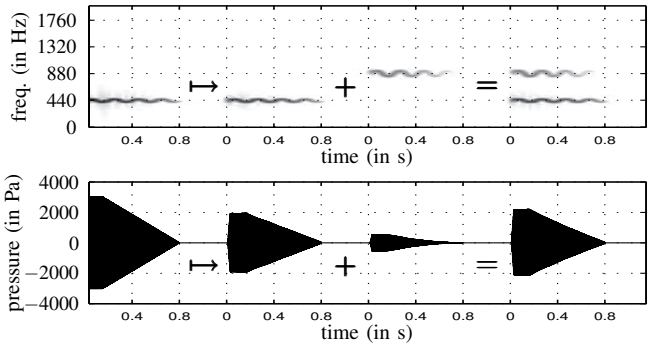

Fig. 11. *Spectrograms and signals of* $p_0 \mapsto y_{h_1} + y_{h_2} = y_{approx}$ *computed using the digital simulation given in Fig. 10. The excitation is* $p_0 = p_0^{(T1)}$.

(decay). When the nonlinearity is activated, the waveform is distorted (see Fig. 12) and, because of the visco-thermal losses, is continuous. There is no third harmonic since the Volterra series is truncated at order 2.

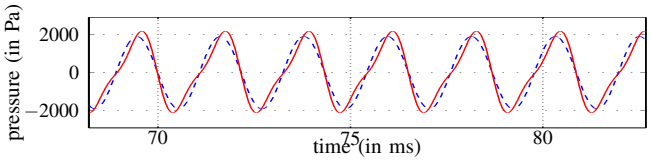

Fig. 12. *Zoom on* $y_{h_1}(t)$ *(linear approximation,*$(--)$*) and on* $y_{h_1}(t)+y_{h_2}(t)$ *(second order approximation,*$(-)$*) obtained for the excitation* $p_0 = p_0^{(T1)}$.

In Fig. 13, $p_0 = p_0^{(T2)}$ is a sound composed of three successive notes of trumpet, the amplitude of which has been tuned to activate the nonlinearity (the mean level is $150\,\mathrm{dB}_{SPL}$). The output yields a quite natural "brassy" sound which follows the level dynamics.

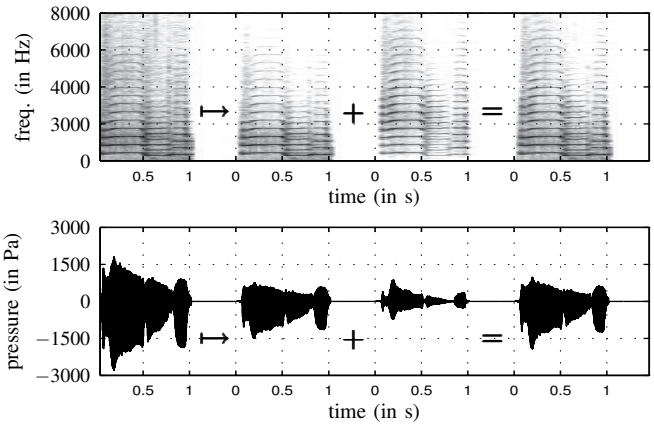

Fig. 13. *Spectrograms and signals of* $p_0 \mapsto y_{h_1} + y_{h_2} = y_{approx}$ *computed using the digital simulation given in Fig. 10. The excitation is* $p_0 = p_0^{(T2)}$.

VII. CONCLUSION

A real-time implementation of the nonlinear propagation in a lossy straight pipe based on Volterra series has been derived. Such an input/output representation is not restricted to stationary signals. But, for the physically realistic model which involves fractional derivatives, identifying a realizable structure from the kernels is not straightforward: contrary to the case of the basic model of absorption, this requires some algebraic manipulations and a decomposition into several elementary sub-systems. Finally, the real-time simulation allows the artificial enhancement and control of the natural brightness of brass sounds. Moreover, this process can be included in sound synthesis based on physical modeling.

From a theoretical point of view, the convergence of the series and the study of the guaranteed error bound due to the truncating should be studied. This requires the generalization of results on ordinary differential equations (see [7]) to the case of the partial differential equations, and to that of some infinite dimensional systems including fractional derivatives. Moreover, comparisons with other methods (e.g. in the case of standing waves) can be performed. Finally, in order to improve the quality of the simulations without increasing the algorithmic complexity, future works will focus on the acceleration of convergence.

ACKNOWLEDGMENTS

The authors thank Remy Muller for his help for the implementation of a VST plug-in which makes real-time audio treatments of sounds possible on many standard home-studio musical softwares.

REFERENCES

[1] J. Gilbert L. Menguy. Weakly non-linear gas oscillations in air-filled tubes; solutions and experiments. *Acta Acustica*, 86:798–810, 2000.

[2] S. Makarov and M. Ochmann. Nonlinear and thermoviscous phenomena in acoustics. Part II. *Acta acustica*, 83:197–222, 1997.

[3] Thomas Hélie and Martin Hasler. Volterra series for solving weakly nonlinear partial differential equations: Application to the Burgers equation with visco-thermal losses. *Int. J. of Control*, 77:1071–1082, 2004.

[4] D. Matignon. Stability properties for generalized fractional differential systems. *ESAIM: Proceedings*, 5:145–158, 1998.

[5] M. Abramowitz and I. A. Stegun. *Handbook of mathematical functions*. Dover, New York, 1970.

[6] M. Hasler. *Phénomènes non linéaires*. École Polytechnique Fédérale de Lausanne, January 1999.

[7] Thomas Hélie and Béatrice Laroche. On the convergence of volterra series of finite dimensional quadratic mimo systems. *International Journal of Control, special issue in Honor of Michel Fliess 60 th-birthday*, 81-3:358–370, 2008.

[8] W. J. Rugh. *Nonlinear System Theory, The Volterra-Wiener Approach*. The Johns Hopkins Univ. Press, 1981.

[9] Thomas Hélie. On the use of volterra series for real-time simulations of weakly nonlinear analog audio devices: application to the moog ladder filter. In *DAFx*, Montréal, Québec, 2006.

[10] V. Smet. Simulation de l'effet de cuivrage dans les instruments à vent. Master's thesis, ENS-Cachan, 2005.

[11] G. Montseny. Diffusive representation of pseudo-differential time-operators. *ESAIM: Proceedings*, 5:159–175, 1998.

[12] Thomas Hélie and Denis Matignon. Representation with poles and cuts for the time-domain simulation of fractional systems and irrational transfer functions. *Journal of Signal Processing*, 86:2516–2528, 2006.

[13] Thomas Hélie and Denis Matignon. Diffusive representations for analyzing and simulating flared acoustic pipes with visco-thermal losses. *Mathematical Models and Methods in Applied Sciences*, 16-4:503–536, 2006.

[14] Thomas Hélie, Denis Matignon, and Rémi Mignot. Criterion design for optimizing low-cost approximations of infinite-dimensional systems: towards efficient real-time simulation. *Int. Journal of Tomography and Statistics*, 7:13–18, 2007.